On the Onset of Self-Organizing Electrohydrodynamic Convection in the Thin-Layer Electrolytic Cells

Marek Orlik[†]

The University of Warsaw, Department of Chemistry, ul. Pasteura 1, 02-093 Warsaw, Poland

Received: February 1, 1999; In Final Form: May 4, 1999

In thin-layer cells, the flow of electrochemical current can induce the low-voltage electrohydrodynamic (EHD) convection. Following previous experimental work with the electrolysis of rubrene in 1,2-dimethoxyethane and theoretical calculations of the formation of driving force for the observed EHD convection, a further development of the numerical model is presented. The onset of convection, caused by an enhancement of local fluctuations of the electric current density, is modelled in terms of coupled equations of electrochemical transports and of the Navier−Stokes equations. The model system consists of the two-dimensional layer of the fluid electrolyzed between two planar electrodes, with the interelectrode distance 100 μm. Simulated velocity distributions prove that the inhomogeneous distribution of local current densities across the solution can give rise to the electroconvection of the fluid. The comparison of numerical results with experimental data is sketched.

1. Introduction

In our previous papers we described the experimental realization[1] and numerical model for the creation of the driving force[2] for the low-voltage electrohydrodynamic (EHD) convection, observed in the thin-layer ($d = 60-300$ μm) cell during electrolysis of saturated solution of rubrene (5,6,11,12-tetraphenylnaphtacene, abbreviated further by R) in 1,2-dimethoxyethane (1,2-DME). This luminescent electroconvective system was originally described by Schaper, Schnedler et al.[3−6] The experimental procedure elaborated by us[1] proved additionally that, in order for the cell to function on a practical level, the cell also required the presence of a $10^{-6}-10^{-5}$ mol dm^{-3} added supporting electrolyte. The ions of this salt ensure (i) the formation of double layers at the electrodes and (ii) the flow of sufficiently large electric current through the solution, by enhancing its conductivity. The self-organized elongated or cellular convective patterns were visualized by the chemiluminescence appearing in places where convective flows of rubrene cations and anions met, which led to recombination of these ions with the generation of a visible light. Figure 1 shows representative examples of such luminescent convective structures observed by us, for different voltages applied. The driving force for this electrohydrodynamic convection was calculated[2] as the product of the local excess charge and the local electric field, existing in the solution during the electrolysis. This model was reduced to a one-dimensional case as it was applied to the state of the system when the fluid was considered still quiescent, and then the characteristics of the system could be assumed uniform along the coordinate parallel to electrode surfaces.

In the present paper I describe a further development of our model, which now includes simulation of the convective motion of the fluid. The driving force for the electroconvection was introduced into the Navier−Stokes (N−S) equation, and the resulting motion of the viscous fluid was obtained. Although full hydrodynamic properties can be reproduced in a three-dimensional space only, such a strict approach requires very long computation time. Therefore, for the purpose of this paper, only a two-dimensional space was considered, as sufficient for modeling of the *basic* hydrodynamic properties of our system, in which convection sets in as a result of the amplification of fluctuations.

Thus, the aim of this paper is to prove, on the basis of model calculations, that the electric force, generated in the thin-layer cell during the low-voltage electrolysis of rubrene in 1,2-dimethoxyethane, can give rise to electroconvection under isothermal conditions.

2. Model

The numerical procedure consists of two principal, coupled modules: (i) electrochemical, for modelling of diffusion, migration, and convection transports of ions and molecules and (ii) hydrodynamic, for modeling of the motion of viscous liquid (Figure 2). At every time step of the simulation, in the electrochemical module the spatial distribution of the driving force is calculated. Using this driving force, in the hydrodynamic module, the distribution of fluid velocity is determined which is then introduced back to electrochemical module and used there for the calculation of convective contribution to all the fluxes. The model system consists of the liquid electrolyte placed between two vertical planar electrodes in a way shown schematically in Figure 3.

The presented numerical procedure was prepared in a possibly simplest way for solving both the transport equations of particles and the Navier−Stokes equations and has been optimized for saving the computation time.

2.1. Electrochemical Module of the Procedure. The electrochemical part of the presented approach is a development of the procedure described in our earlier paper,[2] performed by (i) extension of the model to two-dimensional space and by (ii) adding the convection to previously implemented diffusion and

[†] Fax: +48 22 8225996. E-mail: morlik@chem.uw.edu.pl.

10.1021/jp990352w CCC: $18.00
Published on Web 07/21/1999

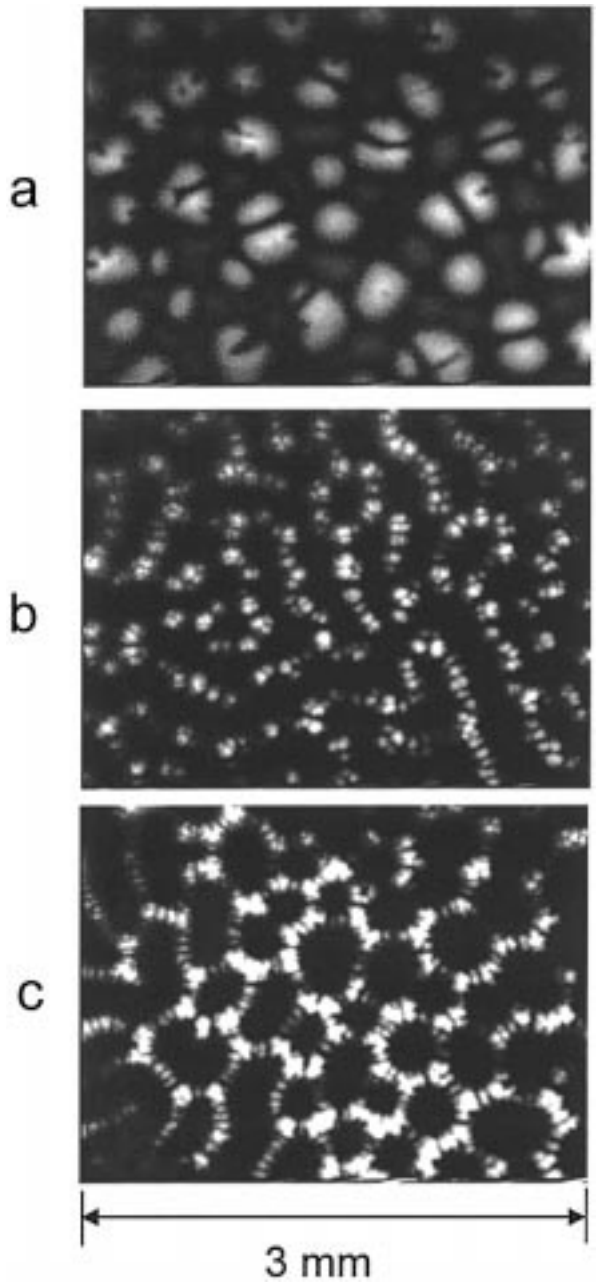

Figure 1. Typical EHD convective patterns of chemiluminescence observed in the thin-layer electrolytic cell, for increasing voltages: (a) $U = 3.0$ V, (b) $U = 3.5$ V, (c) $U = 4.0$ V; the saturated solution of rubrene in 1,2-DME was electrolyzed between the planar Cu cathode and transparent glass anode covered with conducting ITO layer. Concentration of supporting electrolyte (tetrabutylammonium hexafluorophosphate): 7×10^{-6} mol dm^{-3}, interelectrode distance $d = 175$ μm.

migration transports. Thus, the general expression for the vector of the flux of every species (s) now takes a form

$$\mathbf{f}_s = -D_s \nabla c_s - \frac{z_s F D_s}{RT} c_s \nabla\varphi + c_s \vartheta \qquad (1)$$

where c_s and D_s are the concentration and diffusion coefficient of species s; z_s, ionic charges, $z_{R^+} = z_{Cat} = +1$, $z_{R^-} = z_{An} = -1$, $z_R = 0$; φ, electric potential; $\vartheta = [\mathbf{u}, \mathbf{v}]$, the vector of convection velocity; R^+ and R^-, cation and anion of rubrene; Cat and An denote cation and anion of the inert supporting electrolyte, and other symbols have their usual significance.

According to our electrochemical mechanism,[1,2] the *symmetrical* charge injection to the molecules of rubrene at the cathode and at the anode of the thin-layer cell induces the flow of current **I** through the solution. This current is associated with the spatial distribution of the local electric potential gradient ($\nabla\varphi$) in the solution, in dependence on the local concentrations of charge carriers: the appearing ions of rubrene and existing ions of supporting electrolyte. Simultaneously, the divergence of the local electric field (div $\mathbf{E} = -\nabla^2\varphi$) determines the local uncompensated charge density q_{ex} through Poisson's equation:

$$q_{ex}(x,y,t) = -\epsilon\epsilon_0 \nabla^2\varphi = -\epsilon\epsilon_0 \left(\frac{\partial^2\varphi}{\partial x^2} + \frac{\partial^2\varphi}{\partial y^2} \right) \qquad (2)$$

The product of q_{ex} and **E** is equal to the local driving force for electroconvection $\mathbf{F}_{ex}$:

$$\mathbf{F}_{ex} = q_{ex}\mathbf{E} = -q_{ex}\nabla\varphi = \epsilon\epsilon_0 \left(\frac{\partial^2\varphi}{\partial x^2} + \frac{\partial^2\varphi}{\partial y^2} \right) \nabla\varphi \qquad (3)$$

Since in our experimental system the concentration of electroinactive supporting electrolyte is *lower* for more than two orders of magnitude than the concentration of electroactive rubrene molecules ($\sim 4\ 10^{-3}$ mol dm^{-3}), the electric current is controlled *not* by the transport of rubrene molecules to the electrode surfaces but by the conductivity of the solution, dependent on actual concentrations of all ionic species in the interelectrode space.

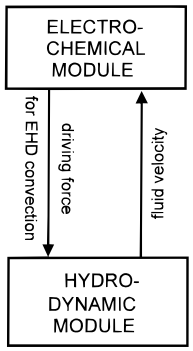

Figure 2. Scheme of the coupling between the electrochemical (transport of particles) and hydrodynamic (fluid motion) modules of the numerical procedure, simulating the onset of electrohydrodynamic (EHD) convection in the thin-layer electrolytic cell.

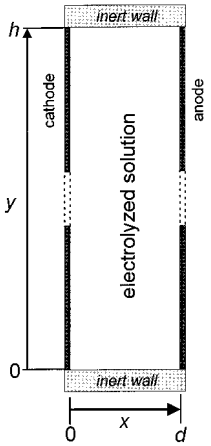

Figure 3. Schematic setup of the modelled electrochemical-convective thin-layer cell; the electrolyzed solution of rubrene and supporting electrolyte in 1,2-DME is placed between the vertical electrodes of a length h and bounded from the top and the bottom by inert, nontransparent walls. Interelectrode distance $d = 100$ μm; the electrode height $h \geq 4d$.

It is further suggested that the local conductivity is largely determined by migration of ions (i.e., ohmic resistance of the solution R), and the contribution from convection, which could lead to the deviation of the behaviour of the system from the ohmic law, is negligible. This conclusion results from the following argumentation. The current density **j**, flowing through the solution, is expressed in terms of the fluxes of all charged (s) particles:[7]

$$\mathbf{j} = F\sum_s z_s \mathbf{f}_s = -F\sum_s z_s D_s \nabla c_s - \frac{F^2}{RT}(\sum_s z_s^2 D_s c_s)\nabla\varphi + F(\sum_s z_s c_s)\vartheta \quad (4)$$

where the most right term in the eq 4 is the product of the velocity of convection ϑ and of the excess charge q_{ex}:

$$F(\sum_s z_s c_s) = q_{ex} \quad (5)$$

For an ideally electroneutral solution, $q_{ex} = 0$, and then the convection does not contribute at all to the conductivity of the solution. For our system, as previous calculations[2] showed, in the absence of rubrene radicals recombination, the maximum local value of q_{ex} may be of the order of only a 0.1−0.2 microcoulombs per cm^{-3}, while the observed[1] convection velocity is of the order of a few mm s^{-1}. Thus the term $q_{ex}\vartheta$ in eq 4 can (only locally) reach the maximum value of about 0.1 μA cm^{-2}. Furthermore, as it will be shown below, the velocities modeled in the present paper do not exceed a few micrometers per second, so the corresponding local value of current density will reach only 10^{-4} μA cm^{-2}. Since experimentally observed[1] current densities are of the order of 0.1−1 mA cm^{-2}, it becomes clear that the contribution of the convective transport of the charged solution to its total conductivity is really negligible.

However, the convection influences the local conductivity *indirectly* in this way that it modifies the spatial distribution of ions in the solution. Consequently, appearing gradients of concentrations (∇c) and of the electric potential ($\nabla\varphi$) cause the splitting of the total current $I = |\mathbf{I}|$ into local components $I_x = j_x A_x$ and $I_y = j_y A_y$ which are interrelated through the principle of charge conservation:

$$\mathrm{div}\ \mathbf{j} = \frac{\partial j_x}{\partial x} + \frac{\partial j_y}{\partial y} = -\frac{\partial q_{ex}}{\partial t} \quad (6)$$

where A_x and A_y are local surface areas, normal to the directions of flow of the appropriate components of the vectors of the current.

One should emphasize here that our experimental system is significantly different from other electro-convective ones, described in the literature (cf. e.g., refs 8−14), for which a high-voltage ($U \geq$ several kV) unipolar or bipolar injection of ions into the *electrolyte-free* solution was reported. In such cases the injected ions conduct the current in all spatial dimensions to a comparable extent, according to the geometry of evolving convective flows. In our case, however, due to the presence of ions of supporting electrolyte, a direction normal to the electrode surfaces (x) is a rather dominating pathway of the flow of current ($I \cong I_x$), while I_y components, resulting from local distortion of the distribution of ionic concentrations and electric potential along the y-coordinate, are rather side ones. This means that in our system the flow of current I_x largely determines the electrochemical and electrostatic features of the system. This principal point of view will be used further for the construction of a numerical algorithm.

Flows Along the x-Direction. The current I_x injected at the interphases is related to the x-components of surface fluxes of rubrene in the following way:

$$I_x(0,y,t) = FA_x[f_{x,R}(0,y,t) + 2f_{x,R^+}(0,y,t)] = -FA_x[f_{x,R^-}(0,y,t) - f_{x,R^+}(0,y,t)] \quad (7)$$

$$I_x(d,y,t) = -FA_x[f_{x,R}(d,y,t) + 2f_{x,R^-}(d,y,t)] = FA_x[f_{x,R^+}(d,y,t) - f_{x,R^-}(d,y,t)] \quad (8)$$

with boundary conditions

$$f_{x,R}(0,y,t) + f_{x,R^+}(0,y,t) + f_{x,R^-}(0,y,t) = 0 \quad (9)$$

$$f_{x,R}(d,y,t) + f_{x,R^+}(d,y,t) + f_{x,R^-}(d,y,t) = 0 \quad (10)$$

which mean that there is no accumulation of rubrene molecules and ions at the electrode surfaces.

The current I_x is dependent on the electrode potentials which are influenced by ohmic drops ($I_x R_x$) in the solution, and therefore, the current has to be calculated as a root of a nonlinear equation (eq 7 or 8), for a given voltage applied and actual total solution resistance R_x between the electrodes, measured along the x-coordinate. For the determination of surface fluxes in eqs 7 and 8 it is necessary to know the values of surface (for $x = 0$ and $x = d$) concentrations of rubrene species (denoted further as $\chi(0,y,t)$, $\chi(d,y,t)$), which are dependent on the individual cathode and the anode potentials in the following way, justified by the electrochemical reversibility of rubrene reactions:

$$E_{cath} = E_1^0 + \frac{RT}{F}\ln\frac{\chi_R(0,y,t)}{\chi_{R^-}(0,y,t)} = E_2^0 + \frac{RT}{F}\ln\frac{\chi_{R^+}(0,y,t)}{\chi_R(0,y,t)} \quad (11)$$

$$E_{anod} = E_2^0 + \frac{RT}{F}\ln\frac{\chi_{R^+}(d,y,t)}{\chi_R(d,y,t)} = E_1^0 + \frac{RT}{F}\ln\frac{\chi_R(d,y,t)}{\chi_{R^-}(d,y,t)} \quad (12)$$

where E_1^0 and E_2^0 are the formal potentials of R/R^- and R^+/R redox couples, respectively. According to our idea of symmetrical charge injection at both electrodes,[1] the individual electrode potentials in eqs 11 and 12 are estimated by the following relationships:[2]

$$E_{cath} = \left[\frac{E_1^0 + E_2^0}{2}\right] - \left[\frac{|U| - |I_x|R_x}{2}\right] \quad (13)$$

$$E_{anod} = \left[\frac{E_1^0 + E_2^0}{2}\right] + \left[\frac{|U| - |I_x|R_x}{2}\right] \quad (14)$$

where ohmic resistance along x-direction R_x is defined in the following way:

$$R_x = \frac{1}{A_x}\int_0^d \frac{dx}{\kappa(x,y)} = \frac{RT}{A_x F^2}\int_0^d \frac{dx}{\sum_s z_s^2 D_s c_s(x,y,t)} \quad (15)$$

Finally, one should note that for ions of a nonelectroactive supporting electrolyte (Cat, An) the individual *surface* fluxes are equal to zero:

$$f_{x,Cat}(0,y,t) = f_{x,An}(0,y,t) = f_{x,Cat}(d,y,t) = f_{x,An}(d,y,t) = 0 \quad (16)$$

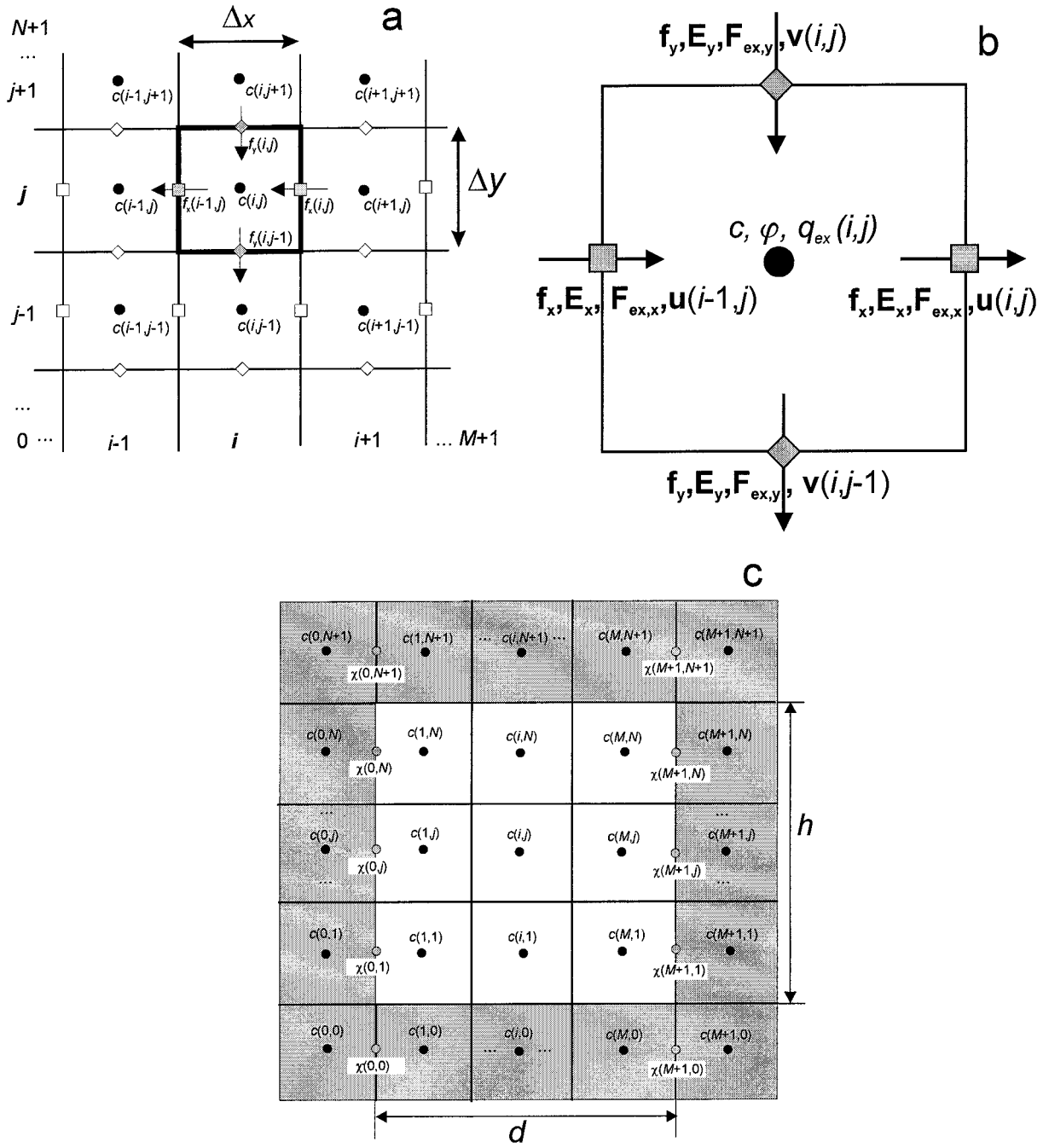

Figure 4. (a) Scheme of discretization of the interelectrode space ($d \times h$) into M intervals $\Delta x = d/M$ along the x-direction and N intervals $\Delta y = h/N$ along the y direction; $c(i,j)$, $i = 1, ..., M$; $j = 1, ..., N$ bulk concentrations calculated at the distances $(i-0.5)\Delta x$, $(j-0.5)\Delta y$; $f_x(i,j)$, $f_y(i,j)$, $i = 0, ..., M$; $j = 0, ..., N$; x- and y-components of the vectors of coupled diffusion, migration, and convection fluxes (cf. eq 1). (b) Enlarged (i,j) spatial cell and its closest environment showing the positions of vectors in the discrete space: fluxes $\mathbf{f}_x$, $\mathbf{f}_y$, electric field $\mathbf{E}_x$, $\mathbf{E}_y$, velocities $\mathbf{u} \equiv \vartheta_x$, $\mathbf{v} \equiv \vartheta_y$ and of scalar quantities: concentrations c, excess charge density q_{ex}, electric potential φ; (c) principle of formulation of boundary conditions for concentrations at the electrode surfaces and inside the virtual external layer (shaded area): $\chi(0,j)$, $\chi(M+1,j)$, concentrations of a given species at the physical electrode surfaces; $c(0,j)$,$c(M+1,j)$—virtual boundary concentrations calculated according to eqs 33 and 34.

Using I_x current, calculated from eq 7 or 8, one can determine the spatial distribution of the electric field $\boldsymbol{E}_x$ across the solution:

$$-\boldsymbol{E}_x(x,y,t) \equiv \frac{\partial \varphi}{\partial x} = \frac{-RT}{F^2 \sum_s z_s^2 D_s c_s}\left[\frac{I_x(x,y,t)}{A} + F\sum_s z_s D_s \frac{\partial c_s}{\partial x}\right] \tag{17}$$

Following the assumption mentioned above that the electrostatic features of the system are largely determined by the current I_x and thus by the electric field along the x direction, the following approximations have been proposed: (i) the distribution of the electric potential $\varphi(x,y,t)$ in the solution can be estimated as

$$\varphi(x,y,t) \cong -E_{cath}(x,y,t) - \int_0^x \boldsymbol{E}_x(x,y,t)\mathrm{d}x \tag{18}$$

where the origin of the φ scale on the x-axis $\varphi(0,y,t)$ has been chosen as equal to $-E_{cath}(x,y,t)$. (ii) since $\partial\varphi/\partial y \ll \partial\varphi/\partial x$, the values of φ obtained from eq 17 were also used for calculations of the resulting vertical gradients $\partial\varphi/\partial y$ for the next time step (Δt) of the discrete simulation procedure. In other words, the

spatial distribution of electrical potential $\varphi(x,y,t)$ was *not* obtained by solving the Poisson's equation $\nabla^2\varphi = -q_{ex}/\epsilon\epsilon_0$ since q_{ex} is not known *a priori* but, conversely, was calculated on the basis of the spatial distribution of the electric field $\boldsymbol{E}_x$ in the electrolyzed solution.

Flows Along the y-Direction. When convection sets in and the composition of the solution along the *y*-coordinate becomes no longer homogeneous, nonzero local gradients of the concentrations of all species, $\partial c_s/\partial y$ and of the electric potential $\partial\varphi/\partial y$ appear, which induce the corresponding flows (fluxes f_y) of the particles. According to the construction of the model system (cf. Figure 3), it should be assumed that all the diffusion and migration fluxes f_y through the lower ($y = 0$) and upper ($y = h$) horizontal inert walls are equal to zero, which corresponds to the von Neumann boundary conditions for the concentrations c_s and the electric potential φ:

$$\left(\frac{\partial c_s}{\partial y}\right)_0 = \left(\frac{\partial c_s}{\partial y}\right)_h = 0 \qquad \text{for} \qquad 0 \le x \le d \quad (19a)$$

$$\left(\frac{\partial \varphi}{\partial y}\right)_0 = \left(\frac{\partial \varphi}{\partial y}\right)_h = 0 \qquad \text{for} \qquad 0 \le x \le d \quad (19b)$$

In the numerical procedure, the small deviations from conditions in eq 19 were used for generation of edge effects at $y = 0$ and $y = h$, which could give rise to the onset of convective motion there.

Furthermore, all the fluxes f_y at the electrode surfaces were assumed as equal to zero:

$$f_{y,s}(0,y,t) = f_{y,s}(d,y,t) = 0 \qquad \text{for} \qquad 0 \le y \le h \quad (20)$$

The latter condition means that surface concentrations of rubrene (and, through electrostatic conditions expressed by the Poisson's equation, also of ions of supporting electrolyte) are determined only by fast and reversible redox equlibria of rubrene at the interphases and not by the side flow of reagents.

In all interior regions of the solution ($0 < y < h$, $0 < x < d$) the nonzero fluxes f_y and associated local I_y currents can develop:

$$f_{y,s}(x,y,t) = -D_s\frac{\partial c_s}{\partial y} - \frac{z_s F D_s c_s}{RT}\frac{\partial \varphi}{\partial y} + c_s v(x,y,t) \quad (21)$$

$$I_y(x,y,t) = -FA_y\sum_s z_s D_s\frac{\partial c_s}{\partial y} - \frac{F^2 A_y}{RT}\left(\sum_s z_s^2 D_s c_s\right)\frac{\partial \varphi}{\partial y} + q_{ex}v \quad (22)$$

In eq 22, as above, the most right, convective contribution is considered negligible, in comparison with the two first right-hand-side terms. When I_y currents begin to flow, the local currents $I_x(x,y,t)$ in the solution undergo a modification to $I'_x(x,y,t)$, according to the principle of conservation of charge (eq 6). Using these improved currents $I'_x(x,y,t)$ one can calculate again a corresponding new distribution of electric field $\mathbf{E}_x$, according to eq 17. The original current $I_x(x,y,t)$, calculated according to eq 7 or 8, keeps its sense as the rate of charge injection at the interphases only and in this way determines the actual boundary conditions.

Summarizing all the above relationships for the *x*- and *y*-directions, the progress of concentration changes of all molecules and ions, as a function of time, is expressed by the general transport equation:

$$\frac{\partial c_s}{\partial t} = -\operatorname{div}\mathbf{f}_s + T_{chem} = -\left(\frac{\partial f_{x,s}}{\partial x} + \frac{\partial f_{y,s}}{\partial y}\right) + T_{chem} \quad (23)$$

where T_{chem} is the kinetic term describing the contribution from chemical recombination of rubrene cationic and anionic radicals, with the regeneration of electroneutral molecules of rubrene.

2.2. Hydrodynamic Module of the Procedure. For the determination of the velocity distribution of the viscous liquid under the influence of the driving force $\mathbf{F}_{ex}$ calculated in the electrochemical module (eq 3), the Navier−Stokes equation was applied. For keeping a convenient compatibility with equations of transports in the electrochemical module, I used the dimensional form of this equation:

$$\frac{\partial \vartheta}{\partial t} + (\vartheta\cdot\nabla)\vartheta = \frac{1}{\rho}[-\nabla p + \eta\nabla^2\vartheta + \mathbf{F}_{ex}] \quad (24)$$

where ρ is the fluid density; η, the coefficient of its dynamical viscosity; and p, pressure evolving in the fluid which was also assumed incompressible:

$$\operatorname{div}\vartheta = 0 \quad (25)$$

The fluid viscosity and density, as well as the temperature $T =$ 298.15 K, were assumed constant what means that eventual side effects originating from thermal convection in the gravitational field were neglected.

Combining eqs 24 and 25, one gets the Navier−Stokes equations in the following final form, suitable for the integration procedure:

$$\frac{\partial u}{\partial t} = \frac{1}{\rho}\left[-\frac{\partial p}{\partial x} + \eta\left(\frac{\partial^2 u}{\partial x^2} + \frac{\partial^2 u}{\partial y^2}\right) + F_{ex,x}\right] - \left[\frac{\partial(u^2)}{\partial x} + \frac{\partial(uv)}{\partial y}\right] \quad (26)$$

$$\frac{\partial v}{\partial t} = \frac{1}{\rho}\left[-\frac{\partial p}{\partial y} + \eta\left(\frac{\partial^2 v}{\partial x^2} + \frac{\partial^2 v}{\partial y^2}\right) + F_{ex,y}\right] - \left[\frac{\partial(v^2)}{\partial y} + \frac{\partial(uv)}{\partial x}\right] \quad (27)$$

where $F_{ex,x}(x,y,t)$ and $F_{ex,y}(x,y,t)$ are the components of the driving force, given by eq 3.

According to the construction of the model system (cf., Figure 3), the boundary conditions for velocity, corresponding to the *immobilization* of the fluid at all boundaries (*no-slip* conditions), take the following form:[15]

$$u(0,y,t) = u(d,y,t) = v(0,y,t) = v(d,y,t) = 0 \qquad y = 0,...,h \quad (28)$$

$$u(x,0,t) = u(x,h,t) = v(x,0,t) = v(x,h,t) = 0 \qquad x = 0,...,d \quad (29)$$

One should note that this physically justified zeroing of all velocity components at the boundaries of the system keeps the surface fluxes in the electrochemical module $f_x(0,j,t)$ and $f_x(d,j,t)$ free of convective contribution, what simplifies corresponding boundary conditions for calculations of current I_x injected at the interphases (cf., eqs 7−12).

For the integration of the Navier−Stokes equations (eqs 26 and 27), the calculation of pressure gradient terms $\partial p/\partial x$ and $\partial p/\partial y$ is necessary, by solving the corresponding Poisson's equation:

$$\left(\frac{\partial^2 p(t+dt)}{\partial x^2}\right) + \left(\frac{\partial^2 p(t+dt)}{\partial y^2}\right) = \left(\frac{\rho}{dt}\right)\left[\frac{\partial F(x,y,t)}{\partial x} + \frac{\partial G(x,y,t)}{\partial y}\right] \quad (30)$$

where quantities F and G are defined as

$$F(x,y,t) = u(x,y,t) + \Delta t\left\{-\left[\frac{\partial(u^2)}{\partial x} + \frac{\partial(uv)}{\partial y}\right] + \frac{1}{\rho}F_{ex,x} + \frac{\eta}{\rho}\left(\frac{\partial^2 u}{\partial x^2} + \frac{\partial^2 u}{\partial y^2}\right)\right\} \quad (31)$$

and

$$G(x,y,t) = v(x,y,t) + \Delta t\left\{-\left[\frac{\partial(uv)}{\partial x} + \frac{\partial(v^2)}{\partial y}\right] + \frac{1}{\rho}F_{ex,y} + \frac{\eta}{\rho}\left(\frac{\partial^2 v}{\partial x^2} + \frac{\partial^2 v}{\partial y^2}\right)\right\} \quad (32)$$

According to the scheme of the coupling between the electrochemical and hydrodynamic modules of the numerical procedures (cf. Figure 2), the calculated x- and y-components of the velocities $u(x,y,t)$ and $v(x,y,t)$ at every time step Δt of the simulation are being introduced back to the convective term of the fluxes (eq 1) in the electrochemical module.

3. Computational Procedure

The finite differences algorithm was used for the integration of both transport equations in the electrochemical module[16−18] and the Navier−Stokes equation in the hydrodynamic module.[15] The schemes of space discretization are however quantitatively different for these modules.

3.1. Scheme of Space Discretization for the Electrochemical Module. For the purposes of the present approach involving a two-dimensional space, the entire region of the interelectrode space has been divided into channels along the directions normal (x) and parallel (y) to electrode surfaces, in a way sketched in Figure 4. For the region of a liquid electrolyte this leads to a set of spatial cells Δx and Δy, characterized by indices $i = 1,...,M$ and $j = 1,...,N$, while electrode surfaces are positioned at $i = 0$ and $i = M + 1$ (cf. Figure 4a). The assignment of different quantities to each cell is done in this way that the scalar (i,j)-quantities are localized in the center of (i,j)-cell, while the x- and y-components of the vector (i,j)-quantities are placed in the center of the upper and of the right-hand-side edges, respectively, of this cell (cf. Figure 4b). Such a way of discretization ensures the convenient compatibility with the space discretization for solving the Navier−Stokes equation in the hydrodynamic module (see below), and for that reason it is slightly different from the scheme of discretization used in our previous paper.[2] One should note that the calculation of x- and y-fluxes involves now different formula at the boundaries (concentration difference divided by distances $\Delta x/2$ or $\Delta y/2$, respectively) and in the bulk (concentration difference divided by entire Δx or Δy step), which corresponds to the formalism of the so-called "box method" of the digital simulation of electrode processes.[16−18] To further enhance compatibility with the space discretization for the Navier−Stokes equations, the *virtual* external layer surrounding the physically existing system was introduced, and corresponding boundary concentrations $c(0,j,l)$ and $c(M+1,j,l)$ were defined in the centers of cells belonging to that layer (cf. Figure 4c). These values are related to the surface concentrations at *physical* electrode/electrolyte boundaries: $\chi(0,j,l)$ and $\chi(M+1,j,l)$ (cf. Figure 4a), obtained from eqs 11 and 12, in a following way, corresponding to the

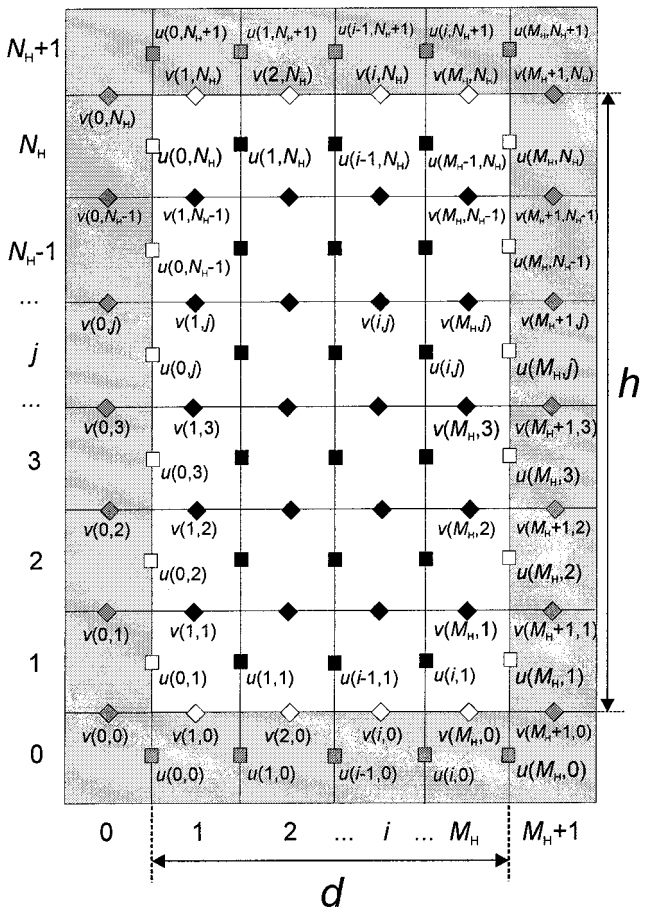

Figure 5. Scheme of space discretization and positions of components of the fluid velocity vectors for the procedure of solving the Navier−Stokes equation; shaded area—virtual layer used for formulation of boundary conditions for velocity components.

Dirichlet boundary conditions:

$$\frac{c(0,j,l) + c(1,j,l)}{2} = \chi(0,j,l) \qquad \text{hence}$$

$$c(0,j,l) = 2\chi(0,j,l) - c(1,j,l) \quad (33)$$

$$\frac{c(M+1,j,l) + c(M,j,l)}{2} = \chi(M+1,j,l) \qquad \text{hence}$$

$$c(M+1,j,l) = 2\chi(M+1,j,l) - c(M,j,l) \quad (34)$$

The boundary conditions along the y-coordinate are treated in an analogous way with the difference being that von Neumann boundary conditions for concentrations and for the electric potential (cf. eq 19) were applied:

$$c(i,0,l) = c(i,1,l) \qquad c(i,N+1,l) = c(i,N,l)$$

$$\varphi(i,0,l) = \varphi(i,1,l) \qquad \varphi(i,N+1,l) = \varphi(i,N,l)$$

$$i = 1,...,M \quad (35)$$

The relations 33−35 were invoked in the numerical procedure at every time step l, before the calculation of the progress of the transports in the x- and y-directions.

3.2. Scheme of Space Discretization for the Hydrodynamic Module. According to the finite differences algorithm, described in ref 15, for integration of the Navier−Stokes equation, the interelectrode space has been divided into finite intervals in a way shown schematically in Figure 5. This way of discretization qualitatively resembles that described above for the electro-

chemical module. However, the resolution of both spatial grids is not necessarily identical, for the following reasons. A successful numerical integration of the equation of *electrochemical* transports of particles, given above, needs the space to be divided into relatively high number of intervals Δx and Δy, i.e., minimum $M = 100$ for the interelectrode distance $d = 100\ \mu$m, and consequently, $N = (h/d)M$ if $\Delta x = \Delta y$. It appears that for the integration of the N−S equation such a fine spatial resolution is highly excessive, since then the computation time increases dramatically for two reasons: (i) the number of equations to be solved significantly rises and (ii) the numerical stability conditions require then appropriately smaller time step Δt. Therefore, for the integration of the N-S equation, the interelectrode space has been divided into M_H space elements Δx_H and N_H space elements Δy_H, *larger*, e.g., by 10 times than Δx and Δy used for the calculations of electrochemical transports. Consequently, at every time step Δt (common for both electrochemical and hydrodynamic modules), the *x*- and *y*-components of the velocities were first determined from the N−S equation at the edges of a very large ($\Delta x_H \times \Delta y_H$) box. Then, by using bilinear interpolation,[15] the velocities at the edges of every small box ($\Delta x \times \Delta y$) of the electrochemical grid were calculated and used in the electrochemical module. The principle of this double space discretization is shown in Figure 6.

According to the space discretization for hydrodynamic calculations, the boundary conditions eqs 28 and 29 now take the following discrete form:

$$u(0,j,l) = u(M_H,j,l) = 0 \quad j = 0, ..., N_H \tag{36}$$

$$v(i,0,l) = v(i,N_H,l) = 0 \quad i = 1, ..., M_H \tag{37}$$

$$u(i,0,l) = -u(i,1,l); \qquad u(i,N_H+1,l) = -u(i,N_H,l) \quad i = 1, ..., M_H \tag{38}$$

$$v(0,j,l) = -v(1,j,l); \qquad v(M_H+1,j,l) = -v(M_H,j,l) \quad j = 1, ..., N_H \tag{39}$$

Equations 38 and 39 mean that these boundary conditions have to be actualized at every time step of the simulation, while two preceding ones keep their initial zero value permanently.

3.3. Difficulties and Simplifications in Calculations. It is well-known that calculations of convective contribution to electrochemical diffusion-migration transports often suffer from stability problems, particularly for relatively high convection velocities. Furthermore, in comparison with modeling of a thermal convection[15] when the temperature is the only quantity involved in transport equations, in the present problem the transport of five kinds of species: rubrene molecules and the cations and anions of rubrene and of the supporting electrolyte, has to be calculated in a way which keeps the concentration balance of all ions concordant with the local excess charge, determined by Poisson's equation. Another source of complications is that the boundary conditions (interfacial potential drops, surface concentrations of all species) are not constant, due to time-dependent local resistance and thus the Ohmic drop in the solution. Moreover, for thermal convection the vector of driving force has only a single component, concordant with the direction of the gravitational field, while in our system electrostatic interactions in the fluid are possible in all spatial directions considered. Finally, the procedure has to work in this way that little fluctuations of solution properties can be amplified, according to the general way in which nonlinear self-organizing phenomena develop.[19] This means the high sensitivity of the course of calculations also for purely numerical "noise" which

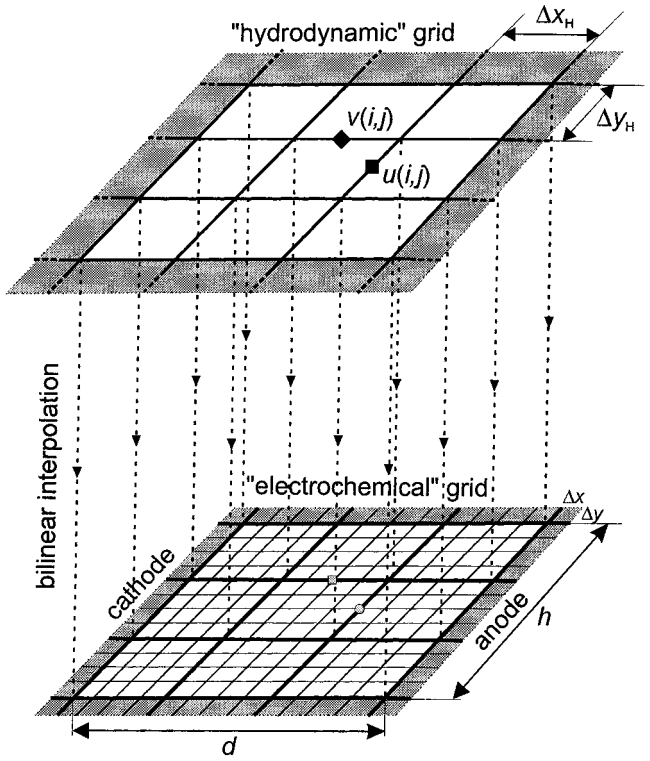

Figure 6. Scheme of superposition of two space grids of different resolution used for the integration of: (i) Navier-Stokes equations (upper layer) and (ii) equations of electrochemical transports (lower layer). The $u \equiv \vartheta_x$ and $v \equiv \vartheta_y$ components of fluid velocities are first calculated at the edges of the upper grid and then interpolated onto the edges of the lower grid.

can destabilize calculations involving so many kinds of transports and species involved. Therefore, the modeling of electroconvection in the system considered requires specific sequence of calculation steps and some reasonable simplifications.

One important simplification, used for the purposes of this particular paper, was neglecting the chemical recombination of rubrene (i.e., $T_{chem} = 0$ in eq 23), a process, which, as it follows from our previous calculations,[2] gives rise to remarkable electric forces at short distances and thus relatively fast local convection. Including this local recombination, which is not decisive for the basic phenomenon of electroconvection in the entire solution, would introduce additional serious stability problems and require very fine discretization of space and time, causing an unreasonable elongation of computation time.

Further simplifications of the electrochemical characteristics of the system have been described and justified in our previous paper.[2] One of those simplification is neglecting the formation of electrical double layers at the electrode/solution interphases. Consequently, in our present model we also neglect the role of eventual electrokinetic phenomena which could occur during the flow of the charged fluid with respect to the solid phase of electrodes.

3.4. Steps of Calculations. Initially, the electrolyzed solution is (i) quiescent (all velocities $u(i,j)$ and $v(i,j)$ equal to zero) and (ii) contains only electroneutral molecules of rubrene and ions of supporting electrolyte. For an enhancement of the numerical stability of the calculations, the progress of diffusion and migration alone was calculated first along the *x*- and then along the *y*-directions. The obtained array of new concentration distribution was then used for calculation of the convective contribution in the *x*- and *y*-directions. The following detailed sequence of calculations involved in a single time loop (for a given time step Δt), was applied.

1. Start from the Electrochemical Module. (i) the actualization of time step Δt, according to the stability condition[15] was

$$\Delta t = \tau \min\left[\frac{\rho}{2\eta}\left(\frac{1}{(\Delta x)^2}+\frac{1}{(\Delta y)^2}\right)^{-1}, \frac{\Delta x}{|u_{\max}|}, \frac{\Delta y}{|v_{\max}|}\right] \quad (40)$$

where the security factor[15] $\tau = 0.5$.

(ii) For every horizontal ($j = 1,...,N$) channel, the following calculation were performed: (a) calculation of the total resistance $R_x(j,l)$;

$$R_x(j,l) = \frac{RT\Delta x}{A_x F^2}\sum_{i=1}^{M}\frac{1}{\sum_s z_s^2 D_s c_s(i,j,l)} \quad (41)$$

(b) calculation of current $I_x(i,j,l)$ injected at the interphases and surface concentrations $\chi(0,j,l)$ and $\chi(M+1,j,l)$ of rubrene ions and molecules (from difference forms of eqs 7 and 8); (c) calculation of the distribution of electric field $\boldsymbol{E}_x(i,j,l)$, along the jth channel:

$$-\boldsymbol{E}_x(i,j,l) \equiv \left[\frac{\Delta\varphi}{\Delta x}\right]_{i,1} = \frac{-2RT}{F^2\sum_s z_s^2 D_s[c_s(i+1,j,l)+c_s(i,j,l)]}\left[\frac{I_x(i,j,l)}{A}+F\sum_s z_s D_s\frac{c_s(i+1,j,l)-c_s(i,j,l)}{\Delta x}\right] \quad (42)$$

(d) calculation of surface concentrations of ions of supporting electrolyte (from the boundary conditions (9, 10, and 16) and Poisson's eq 2), (e) recalculation of surface concentrations $\chi(0,j,l)$ and $\chi(M+1,j,l)$ into $c(0,j,l)$ and $c(M+1,j,l)$ localized inside the virtual external layer (eqs 33 and 34), (f) calculation of the distribution of local electric potential $\varphi(i,j,l)$, along the channel ($i = 1,...,M$),

$$\varphi(i,j,l) = -\left[\frac{E_1^0+E_2^0}{2}-\frac{U-|I_x(i,j,l)|R_x(j,l)}{2}\right]-\Delta x\sum_{k=1}^{i}\boldsymbol{E}_x(k-1,j,l) \quad (43)$$

(iii) For all (i,j) cells of the (x,y) space, the following calculations were performed: (a) calculation of the spatial distribution of local $I_y(i,j)$ currents in the entire (x,y) space:

$$I_y(i,j,l) = -FA_y\sum_s z_s D_s\frac{c_s(i,j+1,l)-c_s(i,j,l)}{\Delta y}-\frac{F^2A_y}{RT}\left(\sum_s z_s^2 D_s\frac{c_s(i,j+1,l)+c_s(i,j,l)}{2}\right)\left(\frac{\varphi(i,j+1,l)-\varphi(i,j,l)}{\Delta y}\right) \quad (44)$$

(b) calculation of the spatial distribution of the new local $I'_x(i,j,l)$ currents, related to the $I_y(i,j,l)$ currents through the principle of the charge conservation, in the entire (x,y) space:

$$I'_x(i,j,l) = I'_x(i-1,j,l)-\left(\frac{A_x}{A_y}\right)\left(\frac{\Delta x}{\Delta y}\right)[I_y(i,j,l)-I_y(i,j-1,l)]+\frac{A_x\Delta x}{\Delta t}[q_{ex}(i,j,l-1)-q_{ex}(i,j,l)] \quad (45)$$

with the boundary value equal to the current injected at the interphases

$$I'_x(0,j,l) = I_x(j,l) \quad (46)$$

(iv) For every horizontal ($j = 1,...,N$) channel, the following calculations were performed: (a) using new local $I'_x(i,j,l)$ currents, determined in iii.b, the calculation of the distribution of the modified $E_x(i,j,l)$ electric field, $i = 1,...,M$ (according to eq 42) and (b) the calculation of the progress of diffusion and migration of all species along the x-direction ($i = 1,...,M$) resulted in the following:

$$c'_s(i,j,l+1) = c_s(i,j,l)-\frac{\Delta t}{\Delta x}[f_{x,s}^{d-m}(i,j,l)-f_{x,s}^{d-m}(i-1,j,l)] \quad (47)$$

where

$$f_{x,s}^{d-m}(i,j,l) = -D_s\frac{c_s(i+1,j,l)-c_s(i,j,l)}{\Delta x}+\frac{z_s F D_s}{RT}\left[\frac{c_s(i+1,j,l)+c_s(i,j,l)}{2}\right]E_x(i,j,l) \quad (48)$$

(v) for every vertical channel ($i = 1,...,M$): using concentration distribution obtained in iv.b, the calculation of the progress of diffusion and migration of all species along the y-direction ($j = 1,...,N$) *resulted in*

$$c''_s(i,j,l+1) = c'_s(i,j,l+1)-\frac{\Delta t}{\Delta y}[f_{y,s}^{d-m}(i,j,l)-f_{y,s}^{d-m}(i,j-1,l)] \quad (49)$$

where

$$f_{y,s}^{d-m}(i,j,l) = -D_s\frac{c_s(i,j+1,l)-c_s(i,j,l)}{\Delta y}-\frac{z_s F D_s}{RT}\left[\frac{c_s(i,j+1,l)+c_s(i,j,l)}{2}\right]\left[\frac{\varphi(i,j+1,l)-\varphi(i,j,l)}{\Delta y}\right] \quad (50)$$

(vi) For all (i,j) cells of the (x,y) space, the following calculations were performed: (a) calculation of the distribution of the local excess charge density $q_{ex}(i,j,l+1)$ from Poisson's equation,

$$q_{ex}(i,j,l) = \epsilon\epsilon_0\left[\frac{E_x(i,j,l)-E_x(i-1,j,l)}{\Delta x}-\frac{\varphi(i,j+1,l)-2\varphi(i,j,l)+\varphi(i,j-1,l)}{(\Delta y)^2}\right] \quad (51)$$

and adjustment of the largest concentration of the ionic species to these q_{ex} values; (b) the calculation of the spatial distribution of driving force for electroconvection,

$$F_{ex,x} = \left[\frac{q_{ex}(i+1,j,l)+q_{ex}(i,j,l)}{2}\right]E_x(i,j,l) \quad (52)$$

$$F_{ex,y} = \left[\frac{q_{ex}(i,j+1,l)+q_{ex}(i,j,l)}{2}\right]\left[\frac{\varphi(i,j+1,l)-\varphi(i,j,l)}{\Delta y}\right] \quad (53)$$

2. Switch to Hydrodynamic Module. (vii) For all (i,j) cells of the (x,y) space, the calculation of velocities $u(i,j)$ and $v(i,j)$

TABLE 1: Model Parameters for Simulation of Electrohydrodynamic Convection in the Thin-Layer Cell, in Which Rubrene Is Electrolyzed in the Presence of Low Amount of Supporting Electrolyte

simulation parameter	symbol	value
temperature	T	298.15 K
interelectrode distance	d	100 μm
electrode height	h	400−600 μm
external voltage	U	4 V
dielectric constant of the solvent (1,2-DME)[27]	ϵ	7.2
dynamic viscosity of the solvent[27]	η	4.55×10^{-4} Ns m^{-2}
density of the solvent[27]	ρ	869.1 kg m^{-3}
bulk rubrene (R) concentration	c_R^0	4×10^{-3} mol dm^{-3}
bulk supporting electrolyte (salt) concentration	c_s^0	1×10^{-5} mol dm^{-3}
formal potential of R/R$^-$	E_1^0	−1.13 V
formal potential of R/R$^+$	E_2^0	+1.37 V
diffusion coefficient of R	D_R	6.2×10^{-6} cm^2 s^{-1}
diffusion coefficient of R$^+$	D_{R^+}	6.2×10^{-6} cm^2 s^{-1}
diffusion coefficient of R$^-$	D_{R^-}	6.2×10^{-6} cm^2 s^{-1}
diffusion coefficient of cation of supporting electrolyte	D_{Cat}	6.2×10^{-6} cm^2 s^{-1}
diffusion coefficient of anion of supporting electrolyte	D_{An}	(a) 6.2×10^{-6} cm^2 s^{-1} (b) 2.8×10^{-5} cm^2 s^{-1}

from the Navier−Stokes equation, at the edges of spatial cells of the hydrodynamic grid ($\Delta x_H \times \Delta y_H$), according to the following relationship:

$$u(i,j,l+1) = F(i,j,l) - \left(\frac{\Delta t}{\rho \Delta x}\right)(p(i+1,j,l+1) - p(i,j,l+1)) \quad i = 1,...,M_H-1, \quad j = 1,...,N_H \tag{54}$$

$$v(i,j,l+1) = G(i,j,l) - \left(\frac{\Delta t}{\rho \Delta y}\right)(p(i,j+1,l+1) - p(i,j,l+1)) \quad i = 1,...,M_H, \quad j = 1,...,N_H-1 \tag{55}$$

where

$$F(i,j,l) = u(i,j,l) + \Delta t\left\{-\left[\left(\frac{\partial(u^2)}{\partial x}\right)_{i,j} + \left(\frac{\partial(uv)}{\partial y}\right)_{i,j}\right] + \frac{1}{\rho}F_{ex,x}(i,j) + \frac{\eta}{\rho}\left(\left(\frac{\partial^2 u}{\partial x^2}\right)_{i,j} + \left(\frac{\partial^2 u}{\partial y^2}\right)_{i,j}\right)\right\} \tag{56}$$

$$G(i,j,l) = v(i,j,l) + \Delta t\left\{-\left[\left(\frac{\partial(uv)}{\partial x}\right)_{i,j} + \left(\frac{\partial(v)^2}{\partial y}\right)_{i,j}\right] + \frac{1}{\rho}F_{ex,y}(i,j) + \frac{\eta}{\rho}\left(\left(\frac{\partial^2 v}{\partial x^2}\right)_{i,j} + \left(\frac{\partial^2 v}{\partial y^2}\right)_{i,j}\right)\right\} \tag{57}$$

and pressures $p(i,j,l+1)$ are found by the iterative solving[15] of Poisson's equation,

$$\frac{p(i+1,j,l+1) - 2p(i,j,l+1) + p(i-1,j,l+1)}{(\Delta x)^2} + \frac{p(i,j+1,l+1) - 2p(i,j,l+1) + p(i,j-1,l+1)}{(\Delta y)^2} = \frac{\rho}{\Delta t}\left[\frac{F(i,j,l) - F(i-1,j,l)}{\Delta x} + \frac{G(i,j,l) - G(i,j-1,l)}{\Delta y}\right] \tag{58}$$

with all the pressures set initially to zero and boundary conditions[15],

$$p(i,0,l) = p(i,1,l); \quad p(i,N_H+1,l) = p(i,N_H,l); \quad i = 1,...,M_H \tag{59}$$

$$p(0,j,l) = p(1,j,l); \quad p(M_H+1,j,l) = p(M_H,j,l); \quad j = 1,...,N_H \tag{60}$$

Exact finite-difference expressions for all terms of the Navier−Stokes equation can be found in Griebel, et al.[15] The discretization involved the mixed weighted (with $\gamma = 0.9$)[15] contribution from the central differences and "donor-cell" scheme ($\gamma = 0$ corresponds to discretization according to pure central differences algorithm, while $\gamma = 1$ switches it to pure "donor-cell" scheme), for all the different forms of the $\partial(u^2)/\partial x$, $\partial(uv)/\partial y$, $\partial(uv)/\partial x$ and $\partial(v^2)/\partial y$ terms.

3. Return to Electrochemical Module. (viii) For all (i,j) cells of the (x,y) space, the following calculations were made: (a) bilinear interpolation of velocities into the edges of spatial cells of the "electrochemical" grid; (b) the calculation of convective contribution to the transport of all species, for the convection along the (x,y), directions, according to the mixed "donor-cell" and "central difference" discretization of the term ($c_s\vartheta$),[15] applied for the enhancement of the numerical stability of the calculations:

$$\begin{aligned} c_s'''(i,j,l+1) = {} & c_s''(i,j,l+1) - \frac{\Delta t}{\Delta x}\left[u(i,j,l)\frac{c_s''(i,j,l) + c_s''(i+1,j,l)}{2} - u(i-1,j,l)\frac{c_s''(i-1,j,l) + c_s''(i,j,l)}{2}\right] \\ & - \frac{\gamma \Delta t}{\Delta x}\left[\left|u(i,j,l)\right|\frac{c_s''(i,j,l) - c_s''(i+1,j,l)}{2} - \left|u(i-1,j,l)\right|\frac{c_s''(i-1,j,l) - c_s''(i,j,l)}{2}\right] \\ & - \frac{\Delta t}{\Delta y}\left[v(i,j,l)\frac{c_s''(i,j,l) + c_s''(i,j+1,l)}{2} - v(i,j-1,l)\frac{c_s''(i,j-1,l) + c_s''(i,j,l)}{2}\right] \\ & - \frac{\gamma \Delta t}{\Delta y}\left[\left|v(i,j,l)\right|\frac{c_s''(i,j,l) - c_s''(i,j+1,l)}{2} - \left|v(i,j-1,l)\right|\frac{c_s''(i,j-1,l) - c_s''(i,j,l)}{2}\right] \end{aligned} \tag{61}$$

where elementary convective fluxes are defined by

$$f_{x,s}^{conv}(i,j,l) = u(i,j,l)\frac{c_s''(i+1,j,l) + c_s''(i,j,l)}{2} \tag{62}$$

$$f_{y,s}^{conv}(i,j,l) = v(i,j,l)\frac{c_s''(i,j+1,l) + c_s''(i,j,l)}{2} \tag{63}$$

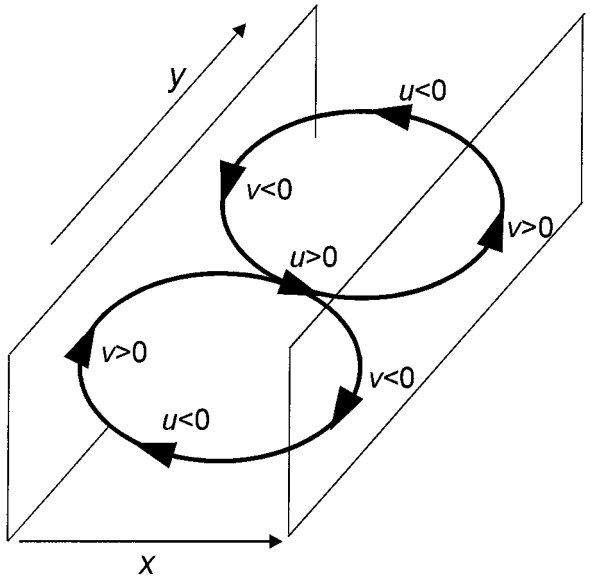

Figure 7. Schematic distribution of *x*- and *y*-components of the fluid velocity $\vartheta = [\mathbf{u}, \mathbf{v}]$ for two cooperating and counter-rotating convective rolls, developed in the interelectrode space.

and, as for the hydrodynamic module, the weighting parameter $\gamma = 0.9$ was chosen.

The following step is to return 1.i through 3.viii until the time loop is completed.

4. Results and Discussion

The *expected* form of the induced self-organized convective motion of the fluid should asymptotically attain a regime of cooperating rolls, of a circular or elliptic cross sections, developing across the entire interelectrode distance. The spatial distribution of velocity components (u,v) for two of such cooperating rolls is sketched in Figure 7.

Let us consider a layer of the electrolyzed solution placed between the cathode and the anode, with the interelectrode distance $d = 100$ μm, electrode height $h = 400-600$ μm, the voltage applied $U = 4$ V, and other parameters as specified in Table 1. Since we found[2] that the different mobilities (diffusion coefficients) of ions are an important factor for the spatial distribution of the driving force for EHD convection, the results will be presented for two cases: (i) when all diffusion coefficients are equal and (ii) when diffusion coefficient of anions of supporting electrolyte is larger than those of all other species.

Calculations for Equal Diffusion Coefficients of All Species. In the initially homogeneous electrochemical thin-layer system, the convection spontaneously starts from the bottom ($y = 0$) and from the top ($y = h$) inert walls of the model system, since only there the situation of the fluid, subject to driving forces, is slightly different from that in the interior region. This small difference which simulates an edge effect, is a result of invoking the von Neumann boundary conditions (eq 35) only once at every time step, before the calculation of transport progress in *x*- and *y*-direction. Then, after the diffusion along the *x*-direction a small difference in concentrations occurs before the channels: ($j = 0$, $j = 1$) and ($j = N$, $j = N+1$) which manifests itself in the progress of edge transports along *y*-direction. At the next time step the boundary conditions (eq 35) equalize edge gradients of concentrations and the electric potential, for enhancing the stability of calculations.

Spatial distribution of convection velocities, shown in Figure 8, proves that at this early stage of the evolution of the motion,

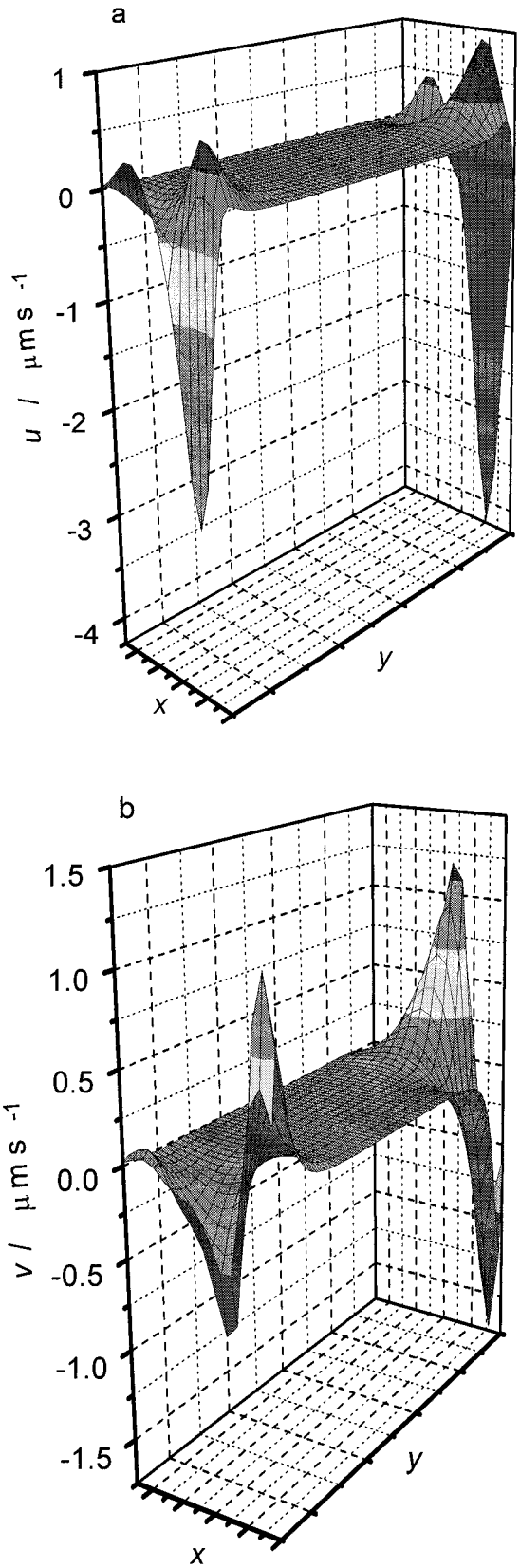

Figure 8. The spontaneous onset of convective motion of the solution at the top and at the bottom inert walls of the system, for model time $t_{obs} = 163$ ms. The motion of solution progresses towards the center. Parameters: $U = 4$ V, $d = 0.01$ cm, $h/d = 4$, $M = 150$, $N = 600$, $(\Delta x_H/\Delta x) = (\Delta y_H/\Delta y) = 10$, all diffusion coefficients equal and other parameters as in Table 1.

at every edge it has a shape of a pair of cooperating rolls of almost circular cross section (with the diameter $\sim d/2$), develop-

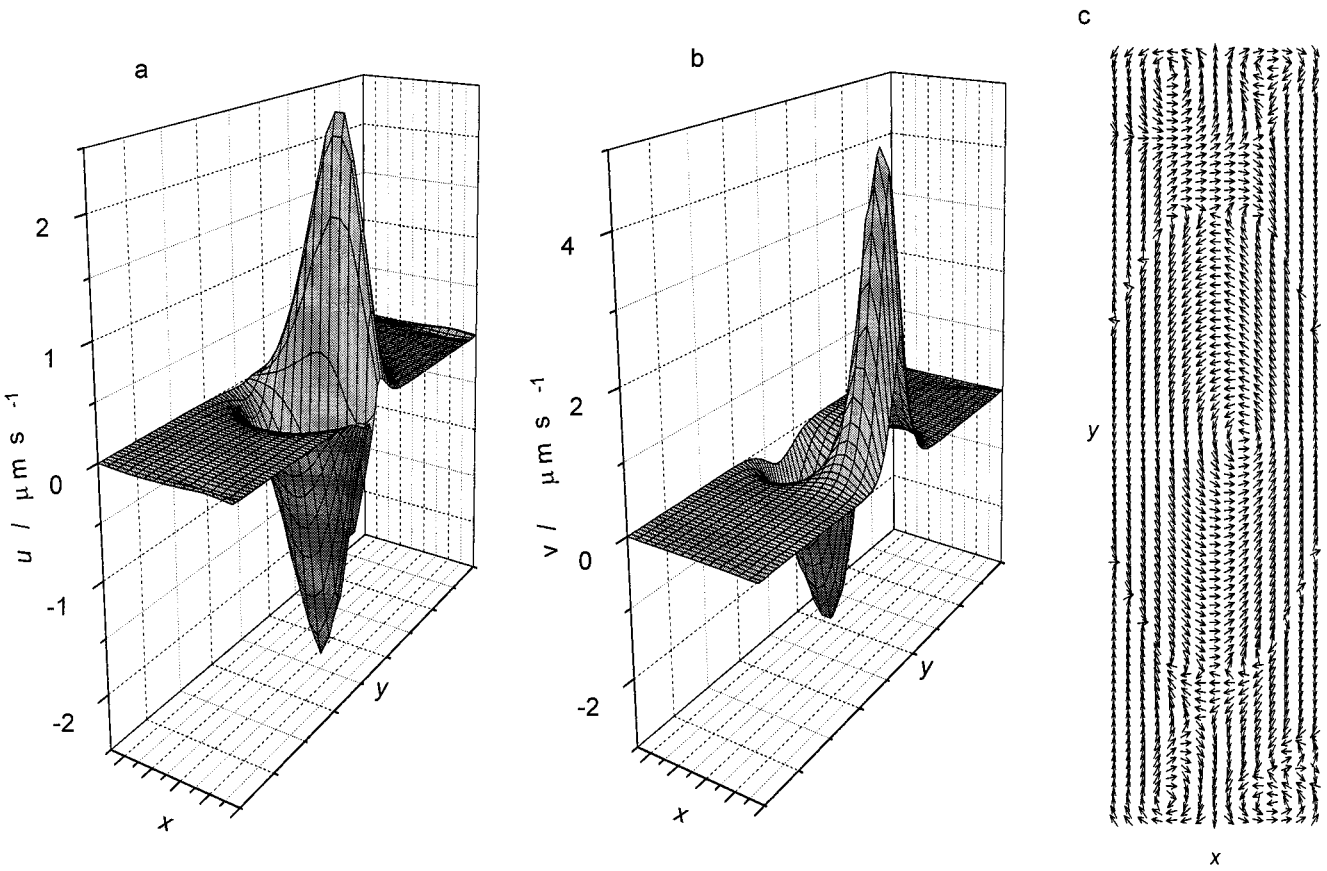

Figure 9. An initial step of evolution of convective motion of the solution observed for model time $t_{obs} = 115$ ms, caused by the single local fluctuation of the ohmic resistance (−1%) introduced in the centre of the solution ($j = N/2$), at time $t_{fl} = 114.7$ ms. The moving solution forms a roll, with the distribution velocity concordant with that predicted by schematic Figure 7. (a) *x*-Component (u), (b) *y*-Component (v) of the total fluid velocity, (c) corresponding vector field of total fluid velocity ϑ. Parameters: $U = 4$ V, $d = 0.01$ cm, $h/d = 6$, $M = 150$, $N = 900$, $(\Delta x_H/\Delta x) = (\Delta y_H/\Delta y) = 10$, all diffusion coefficients equal and other parameters as in Table 1. The position of *y* in (c) indicates the place where the fluctuation was imposed across the solution.

ing between the electrode planes (cf. also Figure 9c for vector representation). Although this motion progresses further towards the center of the solution along the *y*-coordinate, before the entire solution becomes agitated, the increase of a local velocity, developing faster than the progress of motion toward the center of the solution, destabilizes and interrupts numerical calculations.

Since it is difficult to obtain an asymptotic stationary convective regime for such conditions, the role of *intentionally* introduced *bulk* fluctuations in the onset of convection of the fluid was further studied when pattern of non-zero driving forces progressing from the cathode and the anode (cf. Figures 5−7 in ref 2) covered a significant region of the fluid. Thus, at exemplary time $t_{fl} = 114.7$ ms the local, 1% fluctuation of the total solution resistance $R_x(j)$, has been introduced. This fluctuation had a length of the interelectrode distance *d*, the width of the single channel of electrochemical grid (cf. Figures 4 and 6), and was allocated at $y = h/2$ along the coordinate normal to the electrode surfaces (x).

Figure 9 shows that such a local distortion of a current causes a motion of the solution in the form of a roll, expanding over entire layer of the solution. This proves that, according to a general mechanism of nonlinear phenomena, a local fluctuation of current density can be amplified, giving rise to expanding convective motion. Figure 10 shows the corresponding inhomogeneous distribution of local densities of current $j_x(j)$, injected at the interphases.

However, it also becomes clear that modelling for equal diffusion coefficients of all species of rubrene and supporting electrolyte only to a limited extent reproduces the properties of the experimental system, studied by us.

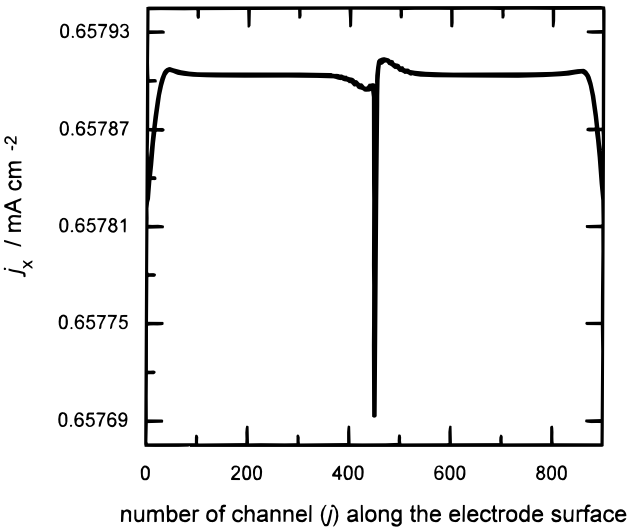

Figure 10. The distribution of current density $j_x(j)$ injected at the interphases, for the conditions listed in the caption to Figure 9. The local decrease of current density in the center of the electrode surface is caused by the imposed increase of local ohmic resistance, while the analogous edge effects correspond to the spontaneous convection induced there (cf. Figure 8).

Calculations for Unequal Diffusion Coefficients of Species. Model conditions, when the diffusion coefficient of the anion

of supporting electrolyte is for the factor of 4.5 higher than diffusion coefficients of all other species, correspond well to the characteristics of our experimental system,[1] containing tetrabutylammonium hexafluorophosphate as added ionic salt. As we showed in our previous paper,[2] a high mobility of anions of supporting electrolyte causes the formation of the pattern of relatively significant driving forces for convection first close to the cathode, which then expand over the entire solution.

One should emphasize that the most striking result of modelling for such properties of supporting electrolyte is that now the spontaneous motion of the fluid develops much better in the form of cooperating rolls expanding in the solution. For visualization of this phenomenon, Figure 11 shows a certain transition step of the evolution of convection of the fluid which starts at the edges and proceeds towards the central region of the solution, in the form of a somewhat drawn-out set of rolls (cf. also Figure 12c for vector representation). One can conclude that, for unequal diffusion coefficients, when driving forces have different values and spatial (now: asymmetric) distribution across the solution, in comparison with those for all diffusion coefficients equal, the progress of convection velocity along the electrode surfaces is faster than the local increase of velocity and therefore the modelling can proceed successfully longer than for all diffusion coefficients equal.

Accordingly, a single imposed fluctuation of the local resistance causes now more distinctly, than for all equal ionic diffusion coefficients (cf. Figure 9), the progress of the self-organizing convection through the solution. Figure 12 shows the transient step of the evolution of such a convection, when the artificially induced central motion of the fluid spreads along the electrode surfaces in this way that the first, centrally formed elliptic roll induces further, neighboring rolls. Particularly, the vector plot (Figure 12c), better than a rather complicated course of *x*- and *y*-components of total fluid velocity (Figure 12a and b), exhibits the directions of these flows. In Conclusion, it is clearly proved that the local fluctuation can result in a set of cooperating rolls.

Comparing vector plots in Figures 9c and 12c one can notice one more interesting difference between the effect of a single central fluctuation on the shape of evolving convective flows. For all equal diffusion coefficients (Figure 9c) a single roll develops and extends around the point belonging to the linear channel of introduced fluctuation, while for the latter case (Figure 12-c) the channel of fluctuation becomes the border between two cooperating, counterrotating rolls.

Finally, one has to mention that also in the case of unequal diffusion coefficients one cannot continue numerical calculations up to an asymptotic stable convective regime. At certain step of calculations the increasing rate of convection leads to destabilization of calculations.

5. Comparison with Experimental Results

Comparison of results of modelling with the experimental results can be focussed on two principal points: (i) the morphology of convective flows and (ii) time scale of evolution of convection.

With respect to point (i), the above numerical results prove, that, particularly for the properties of supporting electrolyte close to those of experimentally applied[1] tetrabutylammonium hexafluorophosphate, the driving force, calculated according to our previously published approach,[2] can give rise to a convective motion of *basic* features (self-organization into roll-like shapes) similar to those reported in the experiment. However, due to troubles with generation of full, steady-state convective struc-

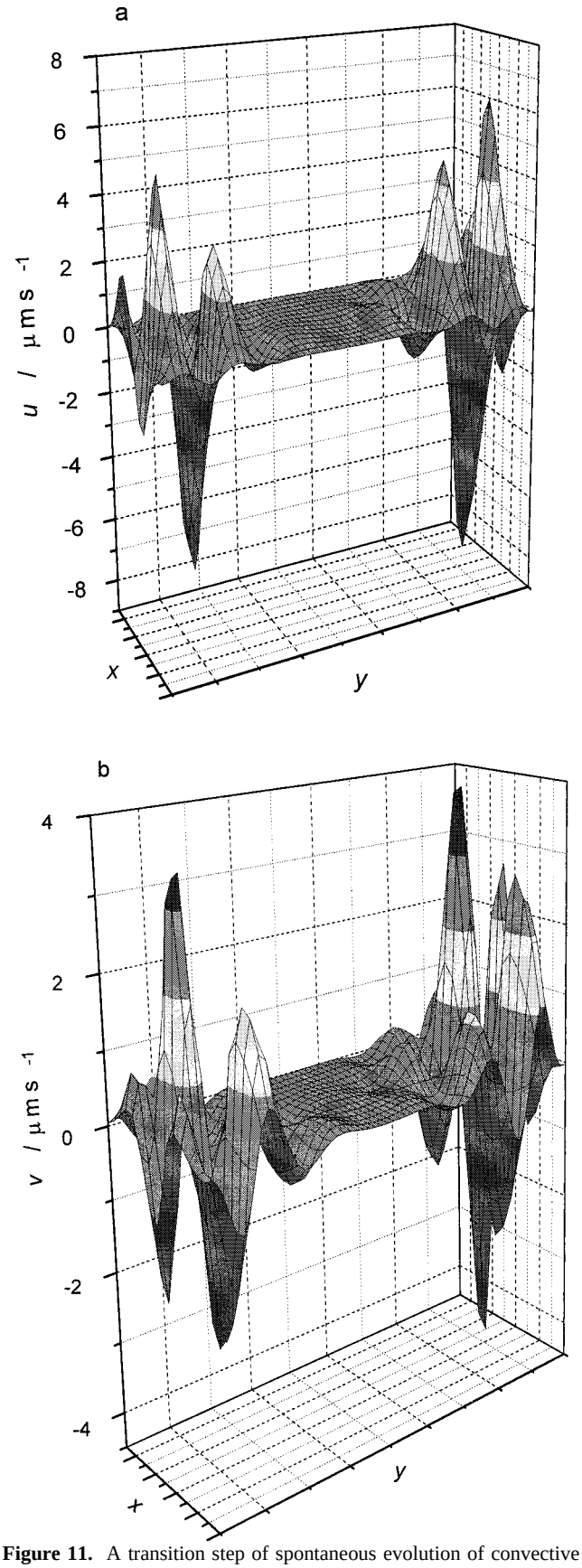

Figure 11. A transition step of spontaneous evolution of convective motion of the solution from its peripheral regions towards the center, for the diffusion coefficient of the anion of supporting electrolyte 4.5 times larger than those of all other species. Model time $t_{obs} = 281$ ms. Specific parameters: $U = 4$ V, $h/d = 4$, $M = 150$, $N = 600$, $(\Delta x_H/\Delta x) = (\Delta y_H/\Delta y) = 10$, $D_{An} = 6.2 \times 10^{-6}$ cm^2 s^{-1}, all other parameters as in Table 1.

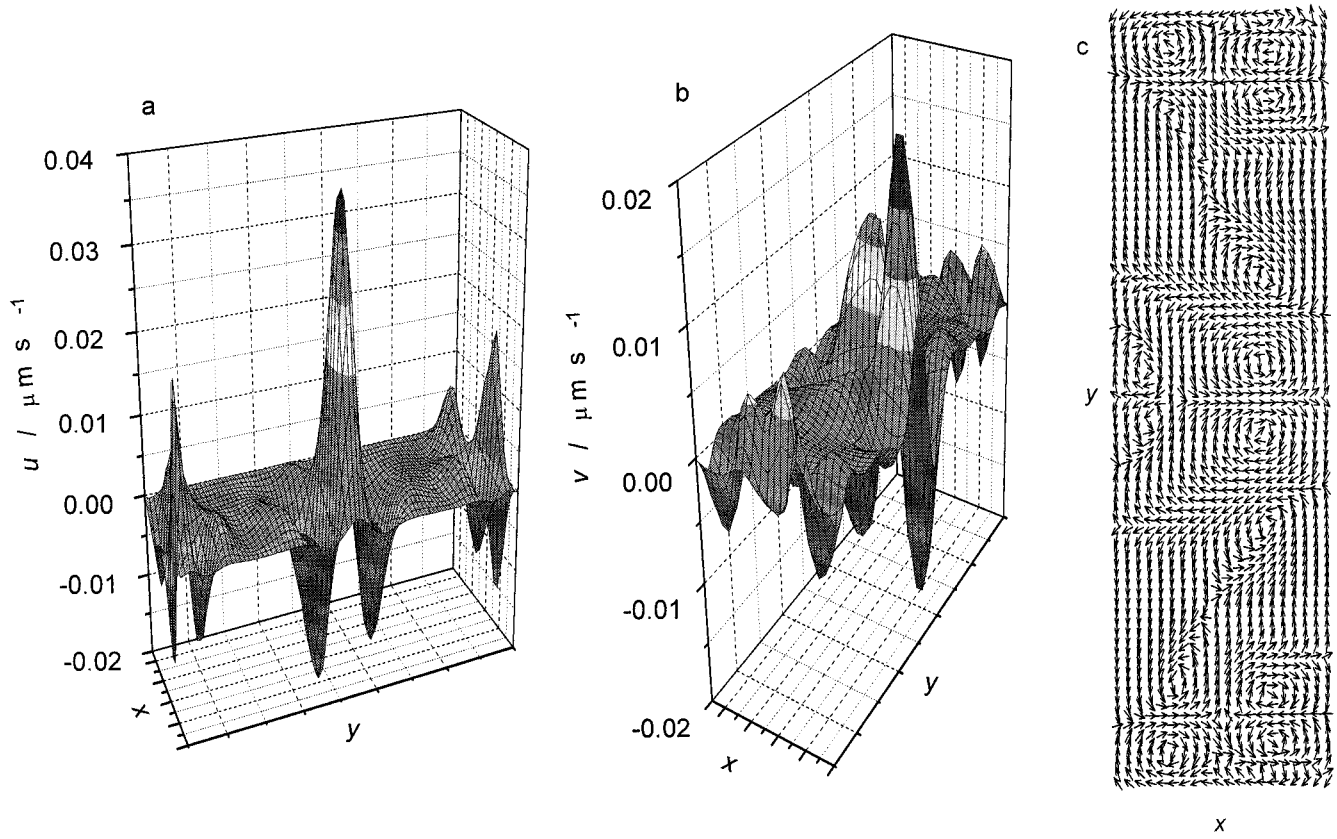

Figure 12. An initial step of evolution of convective motion of the solution observed for model time $t_{obs} = 99.7$ ms, caused by the single local fluctuation of ohmic resistance (−1%) introduced in the centre of the solution ($j = N/2$), at time $t_{fl} = 14.3$ ms. Simultaneously induced spontaneous convection of a comparable velocity, generated at the top and bottom edges of the system, is also visible. (a) *x*-Component (u) and (b) *y*-component (v) of the total fluid velocity, (c) corresponding vector field of total fluid velocity ϑ. The initial couple of counter-rotating convective rolls induces further cooperating rolls of convective motion in the environment. $U = 4$ V, $h/d = 4$, $M = 200$, $N = 800$, $(\Delta x_H/\Delta x) = (\Delta y_H/\Delta y) = 10$, $D_{An} = 6.2 \times 10^{-6}$ cm^2 s^{-1}, all other parameters as in Table 1. The position of letter *y* on Figure (c) indicates the place where the fluctuation was imposed across the solution.

tures at this step of numerical calculations it is not yet possible to compare theoretical and experimental patterns of luminescence. In particular, in terms of the present model it was not possible to establish the maximum asymptotic local velocity, reaching its limiting value for steady-state conditions, as it was observed experimentally[1] and estimated then as of the order of a few mm s^{-1} for typical conditions. I have made additional test calculations of purely hydrodynamic behavior of the 1,2-dimethoxyethane, subject to constant driving forces 3×10^3 N m^{-3} (typical of our electrochemical system), applied in a clockwise way along single rows of the hydrodynamic grid, adjacent to all the walls of the system. For $d = 100$ μm and $h = 400$ μm, the resulting circulating motion of the fluid reached the maximum steady-state local velocity of 0.14 mm s^{-1} and, in principle, velocities of a comparable order of magnitude could be expected also in the electroconvective system studied. The tendency to generate higher local velocities in the model electroconvective system with coupled, electrochemically generated driving forces might then be an artifact which suggests the modification of the simulation algorithm for the enhancement of its numerical stability. The procedures oriented for turbulent flows[15] may appear more appropriate. On the other hand, one should note that if high convection velocities really develop, this can also cause the deviations of the conductivity of the solution from that predicted by Ohm's law.

With respect to point (ii) one has to emphasize first that a very strict comparison of the time scale of evolution of the convection in the model described here and in the experiment is limited, since the dynamics of the double layer formation was not modeled. This introduced a time shift between the model and the experiment comparable to the time constant for charging the double layers, of the order of 16−40 ms (ref 2). Not less important for such a comparison is the fact that our experimental system in which well-defined structures eventually develop was initially *never* ideally homogeneous because of the way in which the solution *had to be* pretreated ("conditioned") by the forced inflow of missing supporting electrolyte from the solution surrounding the interelectrode space.[1] Obviously such a "conditioning" was never ideal and always introduced a certain inhomogeneity (i.e., relatively large fluctuations) in the distribution of the concentration of supporting electrolyte. The role of such established inhomogeneities for the formation of stable convective structures manifested itself as the experimentally observed "memory effect": reproducible distribution of convective structures on electrodes surfaces when the voltage was first switched off and then, after no more than several seconds, switched on again. Obviously the local distribution of ions of supporting electrolyte, established during the formation of self-organized convective flows, remained practically unchanged for the short-time open circuit conditions and this large fluctuation induced the convective flow in the same places, when the voltage was switched on again. Moreover, in the present model the effect of recombination of rubrene ions was neglected, which process additionally significantly influences the spatial distribution of the driving forces.[2] Finally, two other factors can be considered. First, in the present model, only a two-dimensional space was involved what did not allow to reproduce full features of the convective flows. Second, the real properties of the fluid

(especially its viscosity and density) might be different from those for a pure 1,2-dimethoxyethane (cf. Table 1). As the experimental observation of our convective structures showed, the fluid apparently becomes more dense in some places, perhaps due to polymeric species forming on the electrode surfaces, what was also suggested previously by Jaguiro.[26]

Independent of all these limitations, numerical calculations show that the electroconvection self-organizes into cooperating rolls in times less than 1 s, which is roughly concordant with our experimental observations of luminescent patterns for interelectrode distance d less than or equal to approximately 100 μm. For interelectrode distance as large as 200−300 μm this induction time can increase to 2−3 s. This means that the reported electroconvective patterns develop considerably faster than those originating from thermal convection in the gravitational field.[15,19−25]

6. Summary and Conclusions

The model of electrochemical convective system described in this paper proves that the mechanism for the low voltage electrohydrodynamic convection, described qualitatively in our first paper[1] and operating due to driving force calculated according to recently published procedure[2] can explain the spontaneous onset of the motion of the liquid, which leads to convective cooperating rolls. In particular it was shown that local fluctuations of current density constitute a sufficient condition for the onset of the electro-convection in the form of the rolls, according to experimental characteristics of our system, for which inhomogeneous initial distribution of concentration of supporting electrolyte along the electrode surfaces is a consequence of the way in which the sample has to be pretreated for successful development of luminescent convective flows. The modeling of the onset of a self-organized progress of convection was found easier for the diffusion coefficient of anions of the supporting electrolyte larger than for its cations and ions and molecules of rubrene, as for the properties of tetrabutylammonium hexafluorophosphate used in the experiment. These differences in numerical behaviour obtained for equal and unequal diffusion coefficients of ions suggest additional experiments in which our previous results with tetrabutylammonium hexafluorophosphate[1] could be compared with those for another supporting electrolyte of comparable diffusion coefficients of its ions (e.g., tetrabutylammonium tetraphenylborate).

The presented model could be developed further for enhancing the stability of a numerical procedure against relatively high convection velocities, which might lead to a successful modelling of full, stationary convective patterns of luminescence, including effects of recombination of rubrene ions and, if possible, in a three-dimensional space, for which more features of pattern formation in real systems should be reproduced.

Acknowledgment. This work has been partly prepared at the Fritz-Haber-Institut der MPG in Berlin (Germany), during my stay financed by the A. v. Humboldt Foundation (Germany), which is here greatly acknowledged. The author is also grateful for further financial support from BST 592/1/98 project at the Department of Chemistry of the University of Warsaw (Poland) and from the grant KBN/C3840/UW/103/1998 for the part of computer calculations on Convex C3840 computer in the Academic Computer Center "Cyfronet" (Cracow, Poland). Finally, fruitful discussions on the mechanism of electroconvection with Prof. G. Ertl and Dr. K. Doblhofer (FHI, Berlin) are greatly acknowledged.

References and Notes

(1) Orlik, M.; Rosenmund, J.; Doblhofer, K.; Ertl, G. *J. Phys. Chem. B* **1998**, *102*, 1397.

(2) Orlik, M.; Doblhofer, K.; Ertl, G. *J. Phys. Chem. B* **1998**, *102*, 6367.

(3) Köstlin, H.; Schaper, H. *Phys. Lett.* **1980**, *76A*, 455.

(4) Schaper, H.; Köstlin, H.; Schnedler, E. *J. Electrochem. Soc.* **1982**, *129*, 1289.

(5) Schaper, H.; Schnedler, E. *J. Phys. Chem.* **1982**, *86*, 4380.

(6) Schaper, H.; Schnedler, E. *J. Electroanal. Chem.* **1982**, *137*, 39.

(7) Newman, J. S. *Electrochemical Systems*; Prentice-Hall, Inc.: NJ, 1973.

(8) Schneider, J. M.; Watson, P. K. *Phys. Fluids* **1970**, *13*, 1948.

(9) Watson, P. K.; Schneider, J. M.; Till, H. R. *Phys. Fluids* **1970**, *13*, 1955.

(10) Felici, N.; Lacroix, J. C. *J. Electrostat.* **1978**, *5*, 135.

(11) Atten, P.; Lacroix, J. C. *J. Electrostat.* **1978**, *5*, 439.

(12) Lacroix, J. C.; Atten, P. *J. Electrostat.* **1978**, *5*, 453.

(13) Felici, N. *Rev. Gen. Electr.* **1969**, *78*, 717.

(14) Felici, N. *Direct Current* **1972**, *2*, 147.

(15) Griebel, M.; Dornseifer, Th.; Neunhoeffer, T. *Numerische Simulation in der Strömungsmechanik. Eine praxisorientierte Einführung*; Vieweg: Braunschweig/Wiesbaden, 1995.

(16) Feldberg, S. W. In *Electroanalytical Chemistry*; Bard, A. J., Ed.; Marcel Dekker: New York, 1986; Vol. 3, p 199.

(17) Britz, D. *Digital Simulation in Electrochemistry*, 2nd ed.; Springer, Berlin 1988.

(18) Bard, A. J.; Faulkner, L. R. *Electrochemical Methods*; Wiley: New York, 1980 and references cited therein.

(19) Prigogine, I. *From Being to Becoming*; Freeman, NY, 1980.

(20) Bénard, H. *Rev. Gen. Sci. Pures Appl.* **1900**, *12*, 1261, 1309.

(21) Lord Rayleigh *Philos. Mag.* **1916**, *32*, 529.

(22) Chandrasekhar, S. *Hydrodynamic and hydromagnetic stability*, Oxford, 1961.

(23) Küppers, G. Selbstorganisation: Selektion durch Schliessung, In *Chaos und Ordnung. Formen der Selbstorganisation in Natur und Gesellschaft*; Küppers, G., Ed.; Reclam: Stuttgart, 1996.

(24) Bergé, P.; Pomeau Y.; Vidal, C. *Order Within Chaos. Towards a Deterministic Approach to Turbulence*; Wiley-Hermann: Paris, 1984 and references cited therein.

(25) Orlik, M. *Oscillating Reactions. Order and Chaos*; WNT: Warsaw, 1996. In Polish.

(26) Jaguiro, P. Private communication.

(27) Riddick, J. A.; Bunger, W. B.; Sakano, T. K., Eds. *Techniques of Chemistry, Vol. II (Organic Solvents)*, 4th ed.; Wiley: New York, 1986, p 296.